2026 IEEE International Conference on Robotics and Automation (ICRA 2026)
June 1-5, 2026. Vienna, Austria

INTACT-GRIP: An Inflatable Tactile Gripper for Soft Manipulation and High-Resolution Texture Mapping

Ozdemir Can Kara*, Mohammad Rafiee Javazm*, Omid Rezayof, and Farshid Alambeigi

***Abstract*— Robotic manipulation, especially of fragile and irregularly shaped objects, remains a significant challenge due to the need for both adaptability and precise tactile feedback. In this work, we introduce INTACT-GRIP, a robotic gripper that combines soft manipulation and high-resolution tactile sensing for inflation-based soft grasping. INTACT-GRIP integrates inflatable balloons with vision-based tactile feedback, enabling fingertip stiffness modulation for stable and damage-free manipulation of fragile and irregularly shaped objects. To evaluate its performance, we conducted a series of qualitative and quantitative experiments. In these experiments, inflation pressure was manually controlled by a human operator, who adjusted and stopped the pressure based on real-time visual feedback of the captured texture features. The results demonstrate the system's ability to safely conform to fragile and irregularly shaped objects with varying stiffness, enabling pressure-controlled grasping and high-resolution tactile imaging during contact. Furthermore, a case study with a robotic arm highlighted the system's potential as a versatile solution for precise and soft manipulation of delicate objects, supported by pressure-adjustable fingertips and real-time visual–tactile feedback.**

I. INTRODUCTION

Safe and robust manipulation remains a key challenge in robotics, especially when dealing with soft, delicate, or irregularly shaped objects. Traditional manipulation systems typically employ rigid grippers that rely on precisely controlled actuators to secure objects with well-defined geometries [1], [2]. While these rigid grippers can provide excellent precision, payload capacity, and full controllability, they often lack the compliance necessary to handle fragile or deformable items without risking damage [3]–[7]. Comprehensive surveys, such as that by Shintake *et al.* [8], have further classified robotic grippers based on actuation mechanisms and material properties, revealing that while rigid grippers excel in structured environments, their brittleness, high cost, and complexity limit their effectiveness in unstructured settings where unexpected contact is inevitable. These limitations are especially crucial in applications like food handling and delicate manufacturing, where unintended excessive force or misalignment can damage the object.

*These authors contributed equally to this work.

Research reported in this publication was supported by the National Cancer Institute of the National Institutes of Health under Award Number R21CA280747 and Proof of Concept Award in The University of Texas at Austin.

Ozdemir Can Kara, Mohammad Rafiee Javazm, Omid Rezayof, and Farshid Alambeigi are with the Walker Department of Mechanical Engineering, University of Texas at Austin, TX, USA. Email: ozdemirckara@utexas.edu, mr62958@my.utexas.edu, omid.rezayof@utexas.edu farshid.alambeigi@austin.utexas.edu

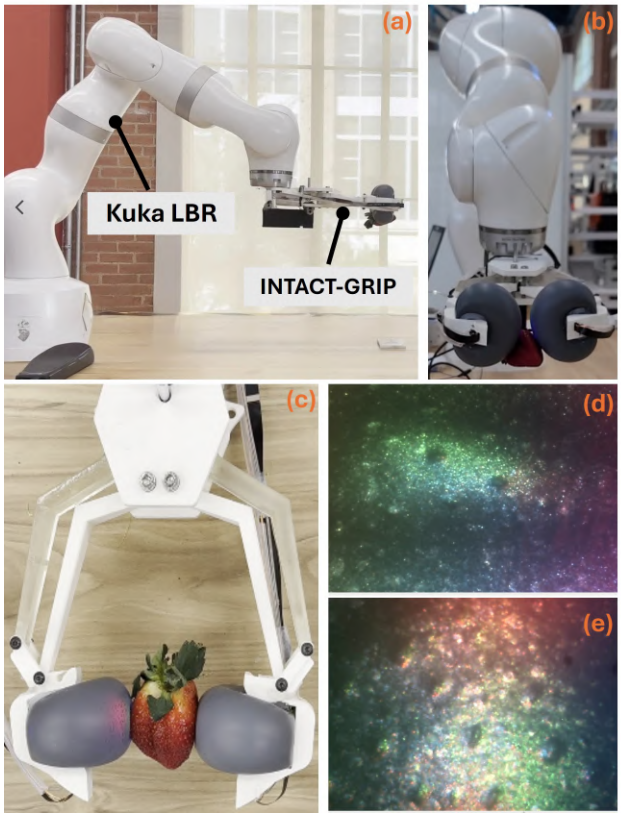

Fig. 1. (a) Integration of INTACT-GRIP with Kuka robotic manipulator while simultaneously obtaining texture images and safely grasping an asymmetrical strawberry; (b) Front and (c) top views of INTACT-GRIP safely gripping the strawberry with two inflated tactile sensing balloons; (d) left- and (e) right-side textural views of strawberry mapped by the inflated balloons of INTACT-GRIP.

In response to these challenges, the robotics community has increasingly turned its attention toward soft robotic grippers. Soft grippers employ compliant materials that inherently provide passive adaptability, allowing them to conform to the contours of irregular and delicate objects [9]–[12]. This design philosophy minimizes the risk of damage while enhancing grasping stability and adaptability. However, most existing soft grippers lack integrated sensing capabilities, which forces them to rely on pre-programmed motion strategies without real-time feedback on the object's properties [13]. This absence of tactile sensing is a significant drawback, as it prevents these systems from dynamically adjusting their grip based on the contact information [4].

To provide tactile feedback for robotic manipulation, vision-based tactile sensors (VBTSs) have become a promising solution for robotic grippers [14]. These sensors (e.g., GelSight [15], Hysense [16], Mint [17]) are made of a

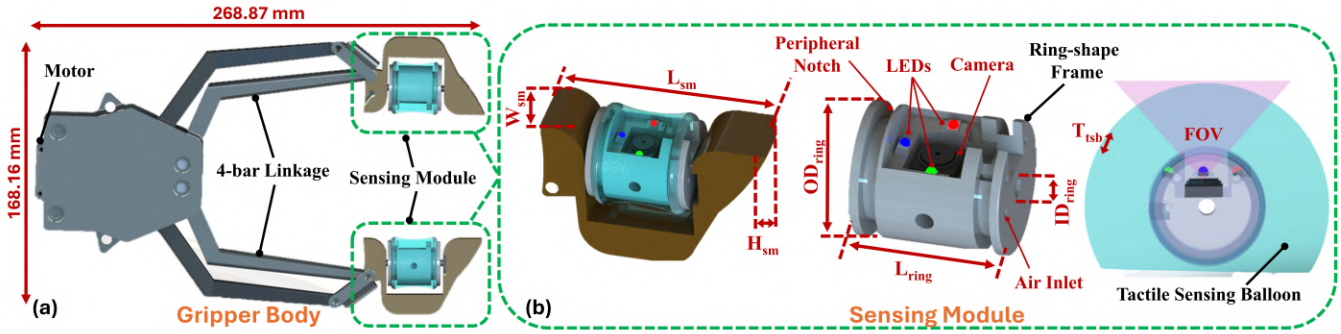

Fig. 2. Design overview of the INTACT-GRIP: (a) Gripper body, (b) Close-up view of the sensing module incorporating ring-shape frame and TSB.

rigid housing attached to a static and deformable elastomer that interacts with an object. These sensors use a camera to capture visual deformations of the deformable elastomer caused by contact forces to provide detailed tactile information of the interacted surface [18]. VBTSs provide significant advantages, including higher spatial resolution, improved sensitivity, and lower manufacturing costs [19]. Despite their potential, VBTSs face challenges, including the rigidity of their structure and the lack of active shape and stiffness adaptation, which limit their ability to conform to objects with complex geometries [20]–[23].

To collectively address the aforementioned challenges in robotic manipulation and vision-based tactile sensing and taking advantage of features offered by soft grippers and VBTSs, in this paper, we introduce *INTACT-GRIP: Inflatable Tactile Gripper for Soft Manipulation and High-Resolution Texture Sensing*. As illustrated in Fig. 1, INTACT-GRIP combines pressure-modulated soft fingertips and vision-based tactile sensing to conform to diverse object geometries while capturing high-resolution texture information during contact. This integration enables user-operated pressure control towards morphology-conforming manipulation, allowing the sensor to physically conform to the object's geometry for secure grasping while capturing high-resolution surface texture information. More specifically, leveraging the vision-based tactile feedback, the pressure of the inflatable soft fingertips are adjusted by the operator to achieve optimal grip. Therefore, the *key contributions* of this work include the design and development of a novel morphing and inflatable vision-based tactile sensor that combines soft robotic adaptation and high-resolution tactile perception in a unified system. Additionally, we present a hybrid manipulation and sensing framework that enables simultaneous grasp adaptation and texture mapping, allowing for an effective handling of delicate objects. To thoroughly evaluate the features of INTACT-GRIP, we performed various experiments on rigid and soft objects with symmetric and asymmetric geometries. Finally, to evaluate the efficacy of the INTACT-GRIP, we integrated it with a KUKA LBR robot arm, where an operator controlled the system to achieve stable gripping and manipulation of a water bottle.

II. INTACT-GRIP Structure

A. Gripper Mechanism

Figure 2 (a) demonstrates the INTACT-GRIP structure consisting of two sensing modules (SMs), a DC motor (XM540-W270, Dynamixel) with dimensions (width $\times$ height $\times$ depth) of 33.5 mm $\times$ 58.5 mm $\times$ 44 mm, and rated torque of 2.12 Nm, and two rigid 4-bar linkage mechanisms, one on each side, with low-friction bearings (606-2RS Uxcell) at the joints to transmit the torques from actuator. This design enables efficient power transmission and precise pinch grasping by aligning the fingertips to face each other during movement. The pinion of the actuator is connected to one side of the outer linkage through the main gear, which then rotates to engage the opposite finger linkage. The gripper body was printed using FDM printer (E2, Raise3D) with ABS. Of note, the gripper body design used in this work is adapted from BaRiFlex Gripper design [24]. We have modified this design to suit the specific requirements of compliant grasping, and to integrate our novel SM structure which has dimensions of 73.50 mm in length (L_{sm}), 22 mm in width (W_{sm}), and 46 mm in height (H_{sm}).

B. Sensing and Deformable Gripping Module

As shown in Fig. 2 (b), the SM consists of two main components: a *ring-shape frame* and a *tactile sensing balloon (TSB)*. The *ring-shape frame* incorporates several essential components: a camera, a soft tactile sensing balloon securely mounted to the frame, three small standard LEDs for interior illumination during balloon inflation, an air pressure inlet for controlling inflation and deflation, and two channels for routing the LED wiring. It also includes two peripheral notches to firmly hold the balloon and prevent air leakage. The length of the ring frame, denoted as L in Fig. 2 (b), was designed to define the sensing area, influenced by the balloon's size, embedded camera, and LEDs. Without loss of generality, based on these design considerations, the following dimensions were chosen: an inner diameter (ID_{Ring}) of 13.2 mm, an outer diameter (OD_{Ring}) of 29 mm, and a frame length (L_{Ring}) of 32.35 mm. A polyurethane tube (TU0212C-20, SMC) was used for inflation and deflation. The frame also houses an 8 MP autofocus USB 2.0 camera module (Arducam IMX219, Uctronics) with a field of view (FOV)

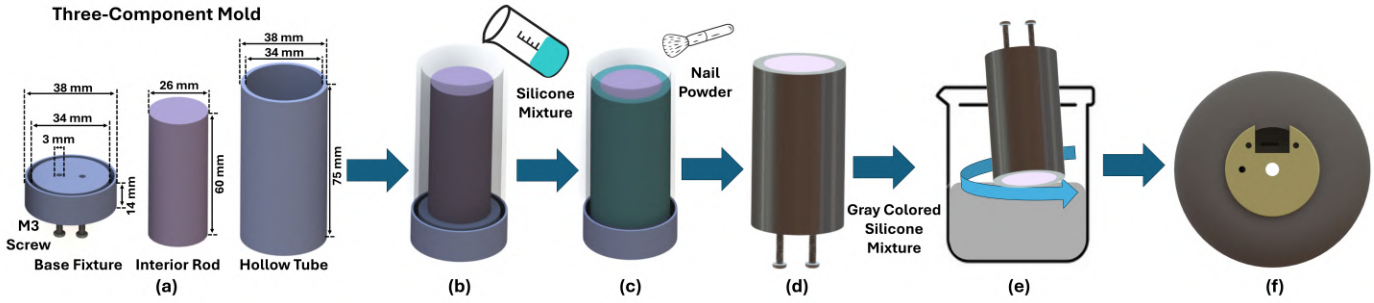

Fig. 3. Fabrication process of the Tactile Sensing Balloon (TSB): (a) A three-component mold is assembled, consisting of a base fixture, an interior circular rod, and a hollow tube. (b) The mold surfaces are treated with a release agent to prevent adhesion. Then, an Ecoflex 00-30 silicone mixture is prepared by mixing Parts A and B in a 1:1 ratio and poured into the mold, filling the space between the hollow tube and the inner rod. (c) After curing at room temperature for 4–5 hours, the outer tube is removed, and reflective nail powder is applied to the silicone surface. (d) The reflective coating enhances the sensor's sensitivity. (e) The coated silicone is then dipped into a gray-pigmented Ecoflex 00-30 mixture, prepared with black and white pigments, and rotated twice during dipping to ensure even coverage. (f) After the final curing stage, the torus-shaped TSB, now integrated with a ring-shaped frame, is ready to be attached to the gripper body.

of 78° (Diagonal) × 60° (Horizontal) × 78° (Vertical), and miniature standard-power Red, Green, and Blue LEDs (941-CLM2DBPCCWAYA453, 941-CLM2DRCCCA0C0BB3, 941-CLM2DGCCCB0F0793). The frame was fabricated using a Stereolithography (SLA) 3D printer (Form 3, Formlabs Inc.).

TSB is essential for creating a flexible, compact, and independently actuated SM that can simultaneously perform tactile sensing and soft manipulation tasks. The sensing component should passively deliver a consistent interaction force and provide high-resolution tactile outputs across the surface of the sensor, enhancing textural mapping when safely interacting with delicate and irregular objects. Simultaneously, this layer should provide sufficient deformability to morph around objects for performing a gripping task. To meet these functional requirements, TSB must replicate the structural and operational functions of the rigid support structures and transparent layers seen in traditional VBTS designs, while also ensuring the proper interaction force and morphability between the sensor and its environment to produce high-quality textural images and gripping.

To effectively solve these interconnected design challenges, three critical criteria must be met: (i) similar to the transparent layer in a conventional VBTS, the balloon material should be sufficiently transparent to ensure clear textural imaging when the inflated INTACT-GRIP interacts with an object; (ii) The internal pressure of the TSB must provide enough stiffness and rigidity, to fulfill the same functional role as the rigid support and plexiglass layers found in standard VBTS systems; (iii) The balloon must be highly stretchable within a defined internal pressure range, appropriate for the target application, allowing adequate radial and lateral expansion to contact and grip the object's surface while maintaining tear resistance and structural integrity. To fully satisfy the design requirements outlined above, a range of materials were evaluated, and Ecoflex 00-30 (Smooth-On Inc.) was chosen for the balloon mechanism fabrication. This translucent silicone was selected for its outstanding mechanical characteristics, such as excellent softness, durability, and remarkable stretchability, which enable it to endure considerable deformation without tearing and to return to its original shape without any distortion.

As summarized in Fig. 3, to fabricate the TSB for the INTACT-GRIP, a three-component mold consisting of a cylindrical outer hollow tube, an interior circular rod, and a base fixture was designed and 3D printed using an FDM printer (Raise 3D Pro2 Series) with Art White PLA filament. The hollow tube had an inner diameter of 34 mm, the rod had an outer diameter of 26 mm, and the mold length was 60 mm. Ecoflex 00-30 silicone (Smooth-On Inc.), mixed in a 1:1 ratio, was used for the balloon. The mold was coated with a release agent (Ease 200) before degassing the silicone mixture in a vacuum chamber. Afterward, the mixture was poured into the mold, filling the space between the tube and rod, and cured at room temperature for 4–5 hours. Once cured, the outer tube was removed, and reflective nail powder was applied to improve sensitivity [25]. A gray-pigmented Ecoflex mixture, containing black and white pigments (Silc Pig, Smooth-On Inc.), was then used to stabilize the reflective layer. The silicone was dipped into the mixture and cured for 6–7 hours. Finally, the balloon with the thickness (T_{tsb}) of 4 mm was detached from the inner rod and ready for attachment to the frame.

III. Evaluation Experiments

To completely validate functionality of INTACT-GRIP for simultaneous safe and soft gripping and texture mapping, we performed the following experiments.

A. Experimental Setup and Procedure

Figure 4 shows the experimental setup designed to evaluate and characterize the performance of a single SM in capturing textural images of different objects under different interaction forces and displacements. The experimental setup includes the SM, various objects (i.e., an M6 screw, a piece of towel, and napkin) with different textures and stiffness levels, a single-row linear stage with 1 μm precision (M-UMR12.40, Newport), and a DC motor (XM430-W350-R,

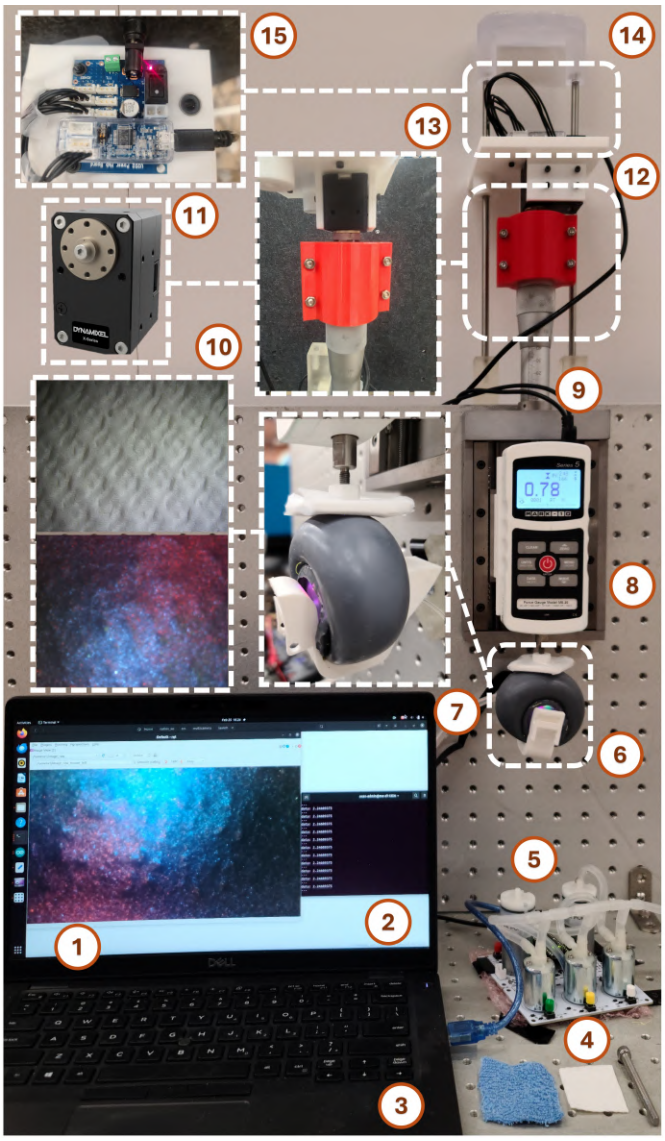

Fig. 4. Overview of the experimental setup: (1) TSB output during the interaction, (2) Real-time pressure screening, (3) PC running ROS for automated experiments, (4) Various objects used in the experiments (e.g., hand towel, napkin, and screw), (5) Programmable Air, (6) Interaction of SM with the napkin, (7) Zoomed-in view of the SM interaction with the napkin at 2.40 kPa, (8) Mark-10 Series 5 Digital Force Gauge, (9) M-UMR12.40 precision linear stage, (10) Zoomed-in view of the napkin with its corresponding SM visual output, (11) Dynamixel DC motor XM430-W350-R, (12) Coupling of DC motor to the linear stage, (13) Close-up view of the DC motor with its coupling, (14) U2D2 power hub, (15) Close-up view of the U2D2 power hub.

Dynamixel) that moves the linear stage over the desired distance. A power hub board (U2D2, Dynamixel) powers the DC motor, while a digital force gauge with 0.02 N resolution (Mark-10 Series 5, Mark-10 Corporation) precisely measures the interaction force. The framework- including streaming, pressure monitoring, stage movement, video recording for image processing, and force measurement- is managed using the Robot Operating System (ROS), which processes the connected USB nodes. A pneumatic actuation system (Programmable Air, Crowd Supply) controls the inflation and deflation of the TSB and monitors the internal balloon pressure to ensure safety. This system consists of two air pumps, three solenoid valves, and an air pressure sensor. All electronics are controlled, and data is collected within the ROS environment.

As shown in Fig. 4, to conduct the experiments, the SM was first secured onto a 3D-printed rigid fixture on the optical table, and an object was attached to the force gauge. The hardware including the SM camera, force gauge, and linear stage motor, was then initialized. Pressure control, force measurements, and camera output visualizations were all managed within the ROS framework to automate the procedure, minimize human error, ensure consistency, and synchronize data recordings. After reaching the desired pressure via the pneumatic system, a customized ROS program collected data as follows: (i) The linear stage motor moved in 0.25 mm increments to interact with the SM; (ii) At each increment, two images were saved, and force was recorded for 10 seconds; (iii) After reaching the target displacement (e.g., 6 mm), the motor reversed and repeated the process. The maximum displacement was limited by the camera's focus distance, as outputs became blurry beyond a certain point. Pressure levels were set based on preliminary tests: if internal pressure fell below 2.30 kPa, the camera's focus distance was short; above 3.30 kPa, the increased TSB stiffness reduced sensor sensitivity. The results are shown in Fig. 5.

B. Static Grasping Tests

To assess the efficacy and performance of INTACT-GRIP in simultaneous grasping and texture mapping, we conducted a series of tests in a static position. As shown in Fig. 6, during these tests, INTACT-GRIP interacted with various objects (i.e., a 3D printed gear, strawberry, ball, and collet) that differed in symmetry and stiffness. The fingertip pressures were manually tuned by a human operator based on object shape and compliance, using real-time visual and tactile feedback from SMs to determine when to stop inflation and achieve stable contact. The left and right camera views captured the tactile feedback from the interaction with both sides of object, while the front and top views illustrated the alignment of the gripper with the objects. By varying the pressure of the SMs, we achieved optimal grasping performance, ensuring high-resolution textural images regardless of the object's shape and stiffness. Fig. 6 summarizes the object features, visual outputs, and the corresponding SM pressures used for grasping. The provided complementary videos clearly shows the performance of robot during these experiments.

C. Case Study: Robotic Grasping

Finally, as shown in Fig. 1 and Fig. 7, the INTACT-GRIP was attached to the end-effector of a 7 degrees-of-freedom robotic arm KUKA LBR Med 7 (KUKA, Germany) to perform realistic grasping and manipulation tasks. Several objects such as a water bottle partially filled with water, and a strawberry were used to perform grasping and manipulation tasks using the robot. For these experiments, the robot was programmed to approach the objects from different angles

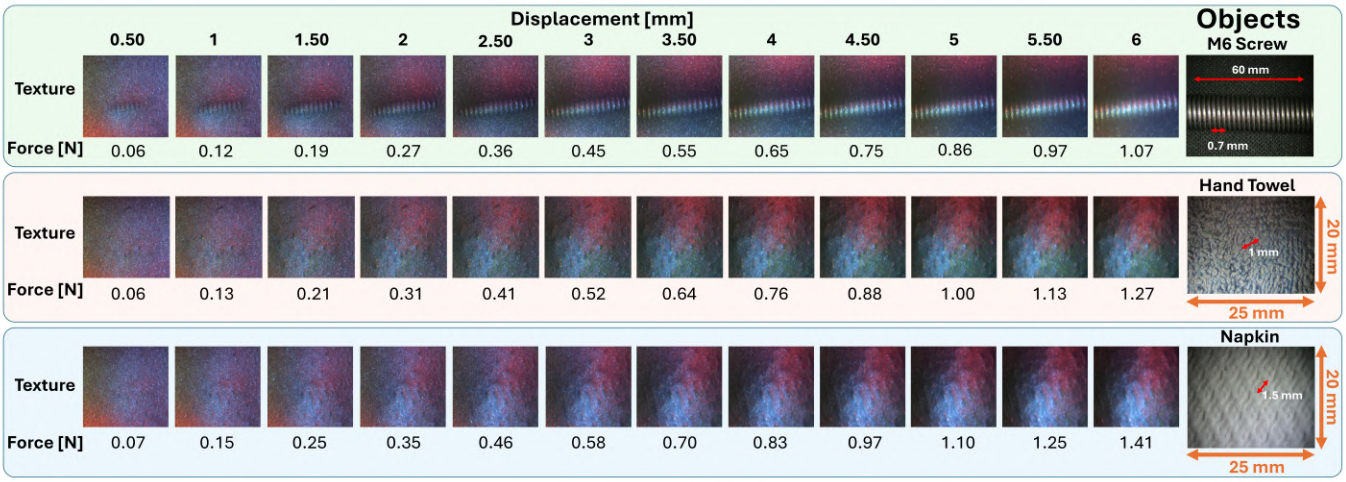

Fig. 5. Visual outputs of the SM during interactions with various objects (screw, hand towel and napkin) at different displacements (0.5 mm to 6 mm) and internal TSB pressure, 2.30 kPa. The dimensions of each object are annotated to illustrate their structural characteristics. The figure illustrates the SM's capability to capture intricate textural and morphological characteristics of objects with different stiffness levels. These results emphasize the sensor's sensitivity, versatility, and effectiveness in detecting subtle textural details and structural differences. Of note, lower pressures produce more detailed texture maps, while higher pressures result in reduced image clarity but improved grasp stability.

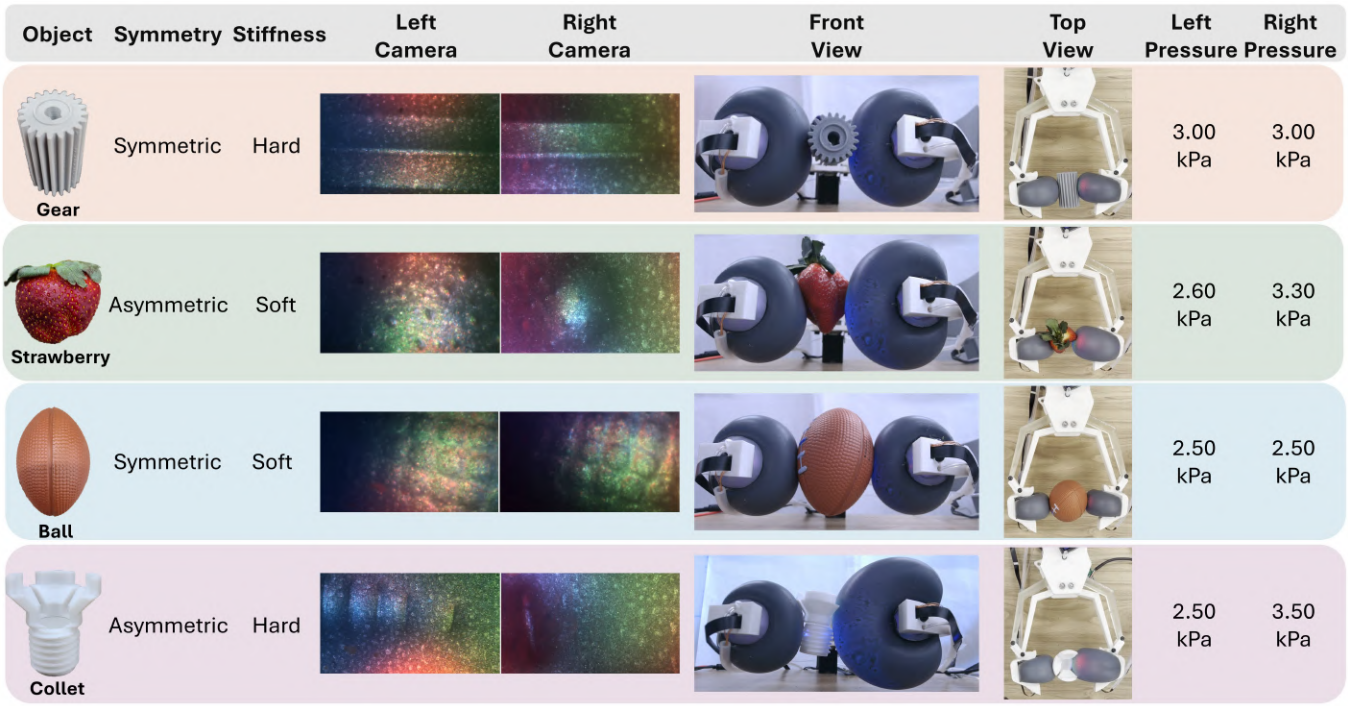

Fig. 6. INTACT-GRIP system interacting with various objects, including a gear, strawberry, ball, and collet, each with different symmetry and stiffness properties. The left and right camera views capture the high-resolution textural information during interaction, while the front and top views show the alignment of the gripper with the objects. The SM pressure is varied to adjust stiffness, demonstrating the system's ability to adapt and provide stable, damage free manipulation of fragile and irregularly shaped objects. In all cases, the inflation pressure was manually controlled by a human operator, who adjusted and stopped inflation based on visual-tactile feedback captured by the sensor.

and different gripping points on the objects (compare Fig. 7 (b) and (f) for the empty bottle and half-empty bottle). During the approaching phase the SMs were deflated (see Fig. 7(a)-(b)). Once the robot reached the target pose, the SMs were inflated and actively adjusted by a human operator using real-time visual and tactile feedback to determine when to stop inflation, ensuring sufficient grip for manipulation (see Fig. 7(c)). Next, the robot was commanded to lift the object (see Fig. 7 (d)). Finally, the robot placed the object on the same spot it was lifted, and approached the object from a different orientation per user's request. No visible damage or deformation was observed on the objects after the tasks, thanks to the soft nature of the SMs. Figure 7 illustrates the robotic and gripper configurations together

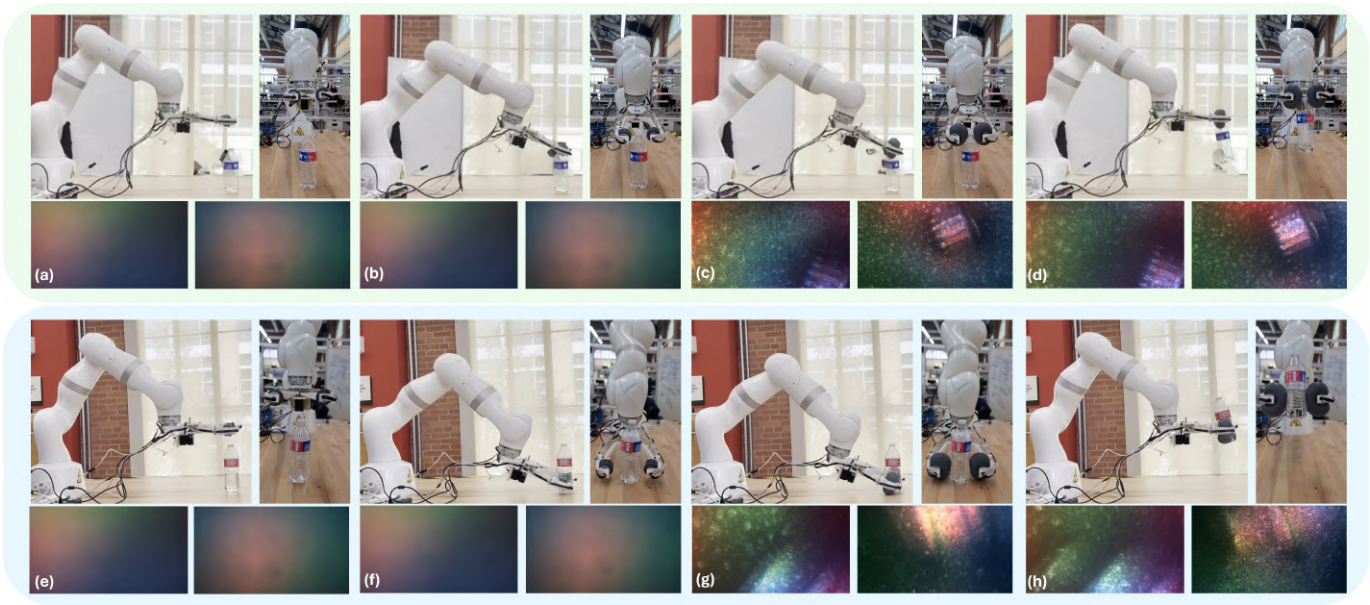

Fig. 7. Integration of INTACT-GRIP with the KUKA LBR robotic arm for manipulation tasks. Subfigures (a-d) show the manipulation of an empty water bottle from the cap, while subfigures (e-h) demonstrate the manipulation of a half-empty water bottle from the bottom. Each sequence includes side and front views, along with corresponding left and right camera textural outputs, capturing the tactile feedback during interaction. The integration of INTACT-GRIP allows precise grasp adaptation and tactile sensing to handle objects with varying contents. Of note, in the performed experiments, the inflation pressure was manually controlled by a human operator, who adjusted and stopped inflation based on visual-tactile feedback captured by the sensor.

with their complementary textural views for two separate trials in which a partially filled water bottle was grasped from its cap (top row) and its bottom (bottom row). The provided complementary videos clearly shows the performance of robot during these experiments.

IV. Results and Discussion

The experimental results demonstrate the efficacy of the INTACT-GRIP, for simultaneous texture mapping and handling objects with varying shapes, textures, and stiffness properties. Fig. 5 illustrates the performance of the INTACT-GRIP system during interactions with different objects, such as a screw, hand towel, and napkin, at various displacements (ranging from 0.5 mm to 6 mm) and a consistent internal pressure of 2.30 kPa. The figure showcases the system's ability to capture intricate textural details (e.g., 0.7 mm features) and surface characteristics of objects with varying stiffness. These results highlight the versatility of the INTACT-GRIP in detecting subtle textural and morphological differences of a paper towel and napkin, which is critical for grasping and manipulating fragile and irregularly shaped items. We observed a consistent trade-off between grasp stability and image clarity. At lower pressures (e.g., 2.3–2.5 kPa), the balloon surface conformed more closely to the object, capturing fine textures such as fabric fibers or screw threads (see Fig. 5, towel and screw). At higher pressures ($>$3.3 kPa), the increased stiffness enhanced contact stability but reduced sensitivity to surface features, resulting in smoother or blurrier images. These observations emphasize the importance of pressure tuning for balancing mechanical grip and tactile sensing quality. It is worth noting that compared with GelSight [15] and similar VBTSs, INTACT-GRIP does not have a rigid transparent layer holding the deformable elastomer of the sensor. Instead by adjusting the inflation pressure, we can provide sufficient rigidity for the TSB and output comparable high-resolution textual images.

Figure 6 demonstrates the INTACT-GRIP's ability to interact with objects of varying symmetry and stiffness, such as a gear, strawberry, ball, and collet. The stiffness of the SM was adjusted by varying the pressure applied, with values ranging from 2.50 kPa to 3.50 kPa, to optimize grasping stability. As shown, the system effectively adapts to objects with different geometric and stiffness properties, providing consistent tactile feedback in both the left and right camera views. For example, when handling the strawberry (as a soft and asymmetric object), the applied pressure was set at 2.60 kPa on the left and 3.30 kPa on the right, ensuring a stable grip while avoiding damage to the object. The corresponding camera views indicate that the SM, with higher pressure, does not capture intricate textural details, as the higher pressure helps achieve a more robust grip on the asymmetric side of the strawberry. Similarly, for the ball (as a soft and symmetric), the pressure was reduced to 2.50 kPa on both sides, allowing the system to maintain a firm grasp without over-compressing the object. This demonstrates the INTACT-GRIP's ability to optimize its grasping performance based on varying object stiffness. Additionally, the asymmetric collet highlights the morphability of INTACT-GRIP during grasping tasks. Table I presents key quantitative metrics of INTACT-GRIP, including its grasping range, pressure and displacement limits, and tactile sensing resolution across all performed experiments.

TABLE I
INTACT-GRIP PERFORMANCE SUMMARY

Metric	Value / Description
Max displacement	6 mm (limited by camera focus)
Pressure range	2.3–3.5 kPa
Grasp force range	∼0.2–1.6 N
Object size range	20–50 mm diameter
Texture resolution	<50 μm features visible

The performed robotic grasping task (as shown in Fig. 7) clearly demonstrates the INTACT-GRIP's ability to adapt and manipulate objects from different locations (e.g., top or bottom) and orientations. The integration with the KUKA LBR robotic arm further highlights INTACT-GRIP's robustness and adaptability for real-world applications, where objects of different weights, contents, stiffness, texture, and shapes need to be manipulated. Also, as clearly shown in Fig. 1, our proposed system is able to also safely manipulate delicate fruits such as a strawberry with an asymmetric geometry while capturing its intricate surface textural features.

V. CONCLUSION AND FUTURE WORK

In this work, we introduced INTACT-GRIP, an inflatable tactile gripper that combines pressure-controlled soft manipulation with high-resolution texture sensing through vision-based tactile feedback. The system effectively bridges the gap between soft robotic flexibility and precise tactile sensing, offering substantial benefits in handling objects with varying stiffness, shape, and texture. Our results demonstrate that INTACT-GRIP enables stable and damage-free manipulation of fragile and irregularly shaped objects, such as strawberries and water bottles, through pressure-controlled compliance. Through the integration of inflatable soft sensors and vision-based tactile sensing, INTACT-GRIP provides enhanced grasping versatility and adaptability, key factors for real-world applications in food handling, fruit picking, and medical robotics.

In the current implementation, internal pressure of INTACT-GRIP was manually regulated by a human operator, who monitored the visual-tactile feedback in real time and determined when to stop inflation to achieve stable contact based on optimal texture mapping. In future work, we plan to address this limitation and automate the system by integrating real-time control algorithms and machine learning techniques to enable adaptive decision-making based on the provided tactile feedback. Specifically, we will focus on automating the pressure control mechanism to dynamically adjust fingertip stiffness in response to contact conditions inferred from visual-tactile data. We also plan to embed INTACT-GRIP within robotic arms to perform more complex manipulation tasks in dynamic and unstructured environments. We will also modify our sensor to simultaneously measure texture and force directly similar to the work proposed in [17].

REFERENCES

[1] J.-H. Bae, S.-W. Park, J.-H. Park, M.-H. Baeg, D. Kim, and S.-R. Oh, "Development of a low cost anthropomorphic robot hand with high capability," in *2012 IEEE/RSJ International Conference on Intelligent Robots and Systems*. IEEE, 2012, pp. 4776–4782.

[2] G. Franchi, A. ten Pas, R. Platt, and S. Panzieri, "The baxter easy-hand: A robot hand that costs $150 us in parts," in *2015 IEEE/RSJ International Conference on Intelligent Robots and Systems (IROS)*. IEEE, 2015, pp. 2917–2922.

[3] L. Li, D. Crosby, M. Shuttleworth, O. F. Argin, A. S. Chen, G. Herrmann, R. Kay, and A. Weightman, "A comparative analysis and scoping review of soft–rigid and industrial parallel rigid grippers," *Advanced Intelligent Systems*, p. 2400503, 2024.

[4] A. Bicchi and V. Kumar, "Robotic grasping and contact: A review," in *Proceedings 2000 ICRA. Millennium conference. IEEE international conference on robotics and automation. Symposia proceedings (Cat. No. 00CH37065)*, vol. 1. IEEE, 2000, pp. 348–353.

[5] A. Bhatia, A. M. Johnson, and M. T. Mason, "Direct drive hands: Force-motion transparency in gripper design," in *Robotics: science and systems*, 2019.

[6] R. Ma and A. Dollar, "Yale openhand project: Optimizing open-source hand designs for ease of fabrication and adoption," *IEEE Robotics & Automation Magazine*, vol. 24, no. 1, pp. 32–40, 2017.

[7] S. Tanaka, K. Koyama, T. Senoo, M. Shimojo, and M. Ishikawa, "High-speed hitting grasping with magripper, a highly backdrivable gripper using magnetic gear and plastic deformation control," in *2020 IEEE/RSJ International Conference on Intelligent Robots and Systems (IROS)*. IEEE, 2020, pp. 9137–9143.

[8] J. Shintake, V. Cacucciolo, D. Floreano, and H. Shea, "Soft robotic grippers," *Advanced materials*, vol. 30, no. 29, p. 1707035, 2018.

[9] E. Navas, R. R. Shamshiri, V. Dworak, C. Weltzien, and R. Fernández, "Soft gripper for small fruits harvesting and pick and place operations," *Frontiers in Robotics and AI*, vol. 10, p. 1330496, 2024.

[10] A. Dzedzickis, J. J. Petronienė, S. Petkevičius, and V. Bučinskas, "Soft grippers in robotics: Progress of last 10 years," *Machines*, vol. 12, no. 12, p. 887, 2024.

[11] N. R. Sinatra, C. B. Teeple, D. M. Vogt, K. K. Parker, D. F. Gruber, and R. J. Wood, "Ultragentle manipulation of delicate structures using a soft robotic gripper," *Science Robotics*, vol. 4, no. 33, p. eaax5425, 2019.

[12] S. Qaddoori Fenjan and S. Fathollahi Dehkordi, "Soft robotic system with continuum manipulator and compliant gripper: design, fabrication, and implementation," in *Actuators*, vol. 13, no. 8. MDPI, 2024, p. 298.

[13] M. Lambeta, P.-W. Chou, S. Tian, B. Yang, B. Maloon, V. R. Most, D. Stroud, R. Santos, A. Byagowi, G. Kammerer, *et al.*, "Digit: A novel design for a low-cost compact high-resolution tactile sensor with application to in-hand manipulation," *IEEE Robotics and Automation Letters*, vol. 5, no. 3, pp. 3838–3845, 2020.

[14] E. Donlon, S. Dong, M. Liu, J. Li, E. Adelson, and A. Rodriguez, "Gelslim: A high-resolution, compact, robust, and calibrated tactile-sensing finger," in *2018 IEEE/RSJ International Conference on Intelligent Robots and Systems (IROS)*. IEEE, 2018, pp. 1927–1934.

[15] W. Yuan, S. Dong, and E. H. Adelson, "Gelsight: High-resolution robot tactile sensors for estimating geometry and force," *Sensors*, vol. 17, no. 12, p. 2762, 2017.

[16] O. C. Kara, N. Ikoma, and F. Alambeigi, "Hysense: A hyper-sensitive and high-fidelity vision-based tactile sensor," in *2022 IEEE Sensors*. IEEE, 2022, pp. 1–4.

[17] M. R. Javazm, S. Kapuria, O. C. Kara, S. Kiehler, R. Hamada, and F. Alambeigi, "Mint: A vision-based soft sensor for mutual integration of normal interaction force and texture perception," in *Proceedings of the IEEE International Conference on Robotics and Automation (ICRA)*, 2026, accepted.

[18] Q. Li, O. Kroemer, Z. Su, F. F. Veiga, M. Kaboli, and H. J. Ritter, "A review of tactile information: Perception and action through touch," *IEEE Transactions on Robotics*, vol. 36, no. 6, pp. 1619–1634, 2020.

[19] O. C. Kara, N. Venkatayogi, N. Ikoma, and F. Alambeigi, "A reliable and sensitive framework for simultaneous type and stage detection of colorectal cancer polyps," *Annals of Biomedical Engineering*, pp. 1–14, 2023.

[20] H. Kim, O. C. Kara, and F. Alambeigi, "A soft and inflatable vision-based tactile sensor for inspection of constrained and confined spaces," *IEEE Sensors Journal*, vol. 23, no. 23, pp. 29 605–29 618, 2023.

[21] O. C. Kara, H. Kim, J. Xue, T. G. Mohanraj, Y. Hirata, N. Ikoma, and F. Alambeigi, "Design and development of a novel soft and inflatable tactile sensing balloon for early diagnosis of colorectal cancer polyps," in *2023 IEEE/RSJ international conference on intelligent robots and systems (IROS)*. IEEE, 2023, pp. 10 295–10 300.

[22] O. C. Kara and F. Alambeigi, "Towards deformation modeling and simulation of a soft and inflatable endoscopic vision-based tactile sensing balloon for cancer diagnosis," in *2025 IEEE/RSJ International Conference on Intelligent Robots and Systems (IROS)*. IEEE, 2025, pp. 1473–1478.

[23] M. R. Javazm, O. C. Kara, and F. Alambeigi, "A novel soft and inflatable strain-based tactile sensing balloon for enhanced diagnosis of colorectal cancer polyps via colonoscopy," *IEEE sensors journal*, vol. 24, no. 16, pp. 26 564–26 573, 2024.

[24] G.-C. Jeong, A. Bahety, G. Pedraza, A. D. Deshpande, and R. Martín-Martín, "Bariflex: A robotic gripper with versatility and collision robustness for robot learning," in *2024 IEEE/RSJ International Conference on Intelligent Robots and Systems (IROS)*. IEEE, 2024, pp. 4106–4113.

[25] S. Zhang, Z. Chen, Y. Gao, W. Wan, J. Shan, H. Xue, F. Sun, Y. Yang, and B. Fang, "Hardware technology of vision-based tactile sensor: A review," *IEEE Sensors Journal*, 2022.